













The McDonald Accelerating Stars Survey (MASS): Discovery of a Long-period Substellar Companion Orbiting the Old Solar Analog HD 47127

Brendan P. Bowler¹ , Michael Endl² , William D. Cochran³ , Phillip J. MacQueen², Justin R. Crepp⁴ , Greg W. Doppmann⁵, Shannon Dulz⁴, Timothy D. Brandt⁶ , G. Mirek Brandt^{6,9} , Yiting Li⁶, Trent J. Dupuy⁷ , Kyle Franson¹, Kaitlin M. Kratter⁸ , Caroline V. Morley¹ , and Yifan Zhou¹ 

¹ Department of Astronomy, The University of Texas at Austin, Austin, TX 78712, USA; bpbowler@astro.as.utexas.edu

² McDonald Observatory and the Department of Astronomy, The University of Texas at Austin, Austin, TX 78712, USA

³ Center for Planetary Systems Habitability and McDonald Observatory, The University of Texas at Austin, Austin, TX 78712, USA

⁴ Department of Physics, University of Notre Dame, 225 Nieuwland Science Hall, Notre Dame, IN 46556, USA

⁵ W.M. Keck Observatory, 65-1120 Mamalahoa Highway, Kamuela, HI 96743, USA

⁶ Department of Physics, University of California, Santa Barbara, Santa Barbara, CA 93106, USA

⁷ Institute for Astronomy, University of Edinburgh, Royal Observatory, Blackford Hill, Edinburgh, EH9 3HJ, UK

⁸ Department of Astronomy, University of Arizona, Tucson, AZ 85721, USA

Received 2021 March 27; revised 2021 April 27; accepted 2021 May 3; published 2021 May 31

Abstract

Brown dwarfs with well-determined ages, luminosities, and masses provide rare but valuable tests of low-temperature atmospheric and evolutionary models. We present the discovery and dynamical mass measurement of a substellar companion to HD 47127, an old ($\approx 7\text{--}10$ Gyr) G5 main-sequence star with a mass similar to the Sun. Radial velocities of the host star with the Harlan J. Smith Telescope uncovered a low-amplitude acceleration of $1.93 \pm 0.08 \text{ m s}^{-1} \text{ yr}^{-1}$ based on 20 years of monitoring. We subsequently recovered a faint ($\Delta H = 13.14 \pm 0.15$ mag) comoving companion at $1''.95$ (52 au) with follow-up Keck/NIRC2 adaptive optics imaging. The radial acceleration of HD 47127 together with its tangential acceleration from Hipparcos and Gaia EDR3 astrometry provide a direct measurement of the three-dimensional acceleration vector of the host star, enabling a dynamical mass constraint for HD 47127 B ($67.5\text{--}177 M_{\text{Jup}}$ at 95% confidence) despite the small fractional orbital coverage of the observations. The absolute H -band magnitude of HD 47127 B is fainter than the benchmark T dwarfs HD 19467 B and Gl 229 B but brighter than Gl 758 B and HD 4113 C, suggesting a late-T spectral type. Altogether the mass limits for HD 47127 B from its dynamical mass and the substellar boundary imply a range of $67\text{--}78 M_{\text{Jup}}$ assuming it is single, although a preference for high masses of $\approx 100 M_{\text{Jup}}$ from dynamical constraints hints at the possibility that HD 47127 B could itself be a binary pair of brown dwarfs or that another massive companion resides closer in. Regardless, HD 47127 B will be an excellent target for more refined orbital and atmospheric characterization in the future.

Unified Astronomy Thesaurus concepts: Brown dwarfs (185); T dwarfs (1679); Companion stars (291); Substellar companion stars (1648)

Supporting material: machine-readable table

1. Introduction

Brown dwarfs and giant planets lack sufficient core temperatures and pressures to stably fuse hydrogen, forcing them to inexorably cool and grow dimmer over time (Kumar 1963). The pace of their evolution is predominantly dictated by their mass but also their accretion history, initial entropy, metallicity, and atmospheric opacity, which varies with wavelength and effective temperature (e.g., Marley et al. 2007; Baraffe et al. 2009; Spiegel & Burrows 2012; Marleau & Cumming 2014). As they cool, substellar objects pass through the L, T, and Y spectral classes, which are defined based on the strength of spectroscopic absorption features in the optical and near-infrared such as FeH, TiO, VO, H₂O, CO, CH₄, and NH₃ (e.g., Kirkpatrick et al. 1999; Burgasser et al. 2006; Cushing et al. 2011). Physically, these features are tied to complex time-dependent chemical and physical processes including grain formation, rain out of condensates, vertical mixing, and chemical disequilibrium (e.g., Ackerman & Marley 2001; Helling et al. 2008; Morley et al. 2012). These atmospheric phenomena in turn affect thermal evolution by acting as surface

boundary conditions for interior structure models. Because so many factors can influence substellar evolution, there is a critical need to empirically validate low-temperature cooling models across a wide range of masses and ages. This is especially urgent because of their regular use to infer the masses of directly imaged exoplanets (Bowler 2016).

Brown dwarfs with dynamically measured masses are among the most valuable tools to test evolutionary models. One approach is to patiently monitor the orbits of brown dwarf binaries; for example, the first binary T dwarf with a dynamical mass revealed early discrepancies between the properties inferred from atmospheric models and those of evolutionary models (Liu et al. 2008). Similarly, Konopacky et al. (2010) found that widely used evolutionary models both systematically under- and overpredict the masses of ultracool dwarfs, and Dupuy & Liu (2017) found that hybrid evolutionary models developed by Saumon & Marley (2008) in which clouds dissipate at the L/T transition are most consistent with coevality tests. When masses *and* ages are both independently constrained, as in the case of brown dwarf companions to stars, evolutionary models can be directly tested (e.g., Dupuy et al. 2009, 2014; Bowler et al. 2018; Brandt et al. 2019). About 15

⁹ NSF Graduate Research Fellow.

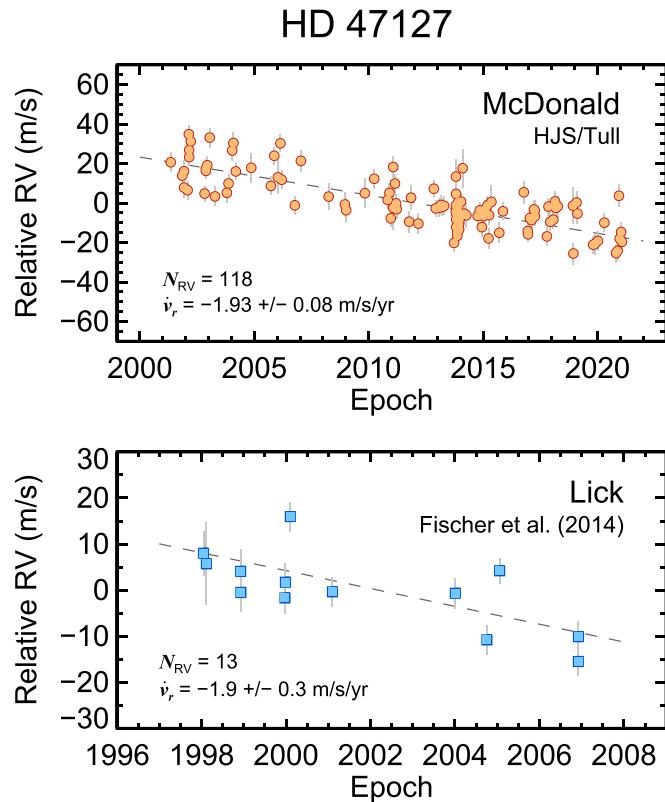


Figure 1. Radial velocities from McDonald Observatory (top) and Lick Observatory (bottom). Both data sets show a shallow radial acceleration of $\approx -1.9 \text{ m s}^{-1} \text{ yr}^{-1}$.

dynamical masses of substellar companions have been measured, only 6 of which are for T dwarfs.

Brown dwarf companions with well-determined orbits are also valuable to probe the formation route of these objects as a population. Bowler et al. (2020) found that the orbits of directly imaged giant planets between 5 and 100 au are significantly more circular compared to brown dwarf companions, which peak at eccentricities of ≈ 0.6 – 0.9 and more closely resemble the orbital properties of wide stellar binaries. However, these results were based on a sample of 27 objects (9 giant planets and 18 brown dwarfs); more examples are needed to address nuanced questions about how eccentricities might vary with age and stellar host mass. Fortunately, several recent and ongoing programs are using stellar accelerations from long-baseline radial velocity (RV) surveys and astrometry from Hipparcos and Gaia to identify new benchmark brown dwarf companions whose orbits can be well constrained (e.g., Crepp et al. 2014; Currie et al. 2020; Maire et al. 2020; Rickman et al. 2020).

Here we present the direct-imaging discovery of a substellar companion to HD 47127, a Sun-like G5 main-sequence star (Adams et al. 1935) located at a distance of 26.62 ± 0.02 pc (based on Gaia EDR3; Gaia Collaboration et al. 2021). HD 47127 is slightly metal-rich ($[\text{Fe}/\text{H}] = +0.1$ dex; Valenti & Fischer 2005) with a mass of $1.02 \pm 0.05 M_{\odot}$ (Luck 2017). It is also inactive and old: Isaacson & Fischer (2010) find a $\log R'_{HK}$ value of -4.984 dex and Wright et al. (2004) measure a value of -5.02 dex; both imply an age of ≈ 6.3 – 7.0 Gyr using empirically calibrated age–activity relations from Mamajek & Hillenbrand (2008) and an age of 8.7 ± 3.2 Gyr (with a 95% CI between 2.7 and 13 Gyr) using BAFFLES, a Bayesian-based

Table 1
Tull Spectrograph Relative Radial Velocities of HD47127

Date (BJD)	RV (m s^{-1})	σ_{RV} (m s^{-1})
2452037.59844	20.7	5.0
2452221.93066	13.9	3.8
2452248.87150	16.1	5.6
2452249.85430	7.8	5.2
2452306.76529	6.5	4.7
2452326.70915	34.9	4.3
2452330.68521	26.8	4.3
2452331.66394	23.3	4.2
2452357.65539	31.2	4.5
2452577.97230	4.8	4.0
...

(This table is available in its entirety in machine-readable form.)

age-dating tool (Stanford-Moore et al. 2020). This is in good agreement with isochronal ages of $9.0^{+3.8}_{-1.7}$ Gyr from the Geneva–Copenhagen Survey of the Solar Neighborhood (Nordstrom et al. 2004) and $7.8^{+3.0}_{-3.7}$ Gyr from Valenti & Fischer (2005). The $v \sin i$ value for HD 47127 is 1.8 km s^{-1} (Glebocki & Gnacinski 2005), consistent with it being a slow rotator with a long rotation period.

The first sign that HD 47127 harbors a wide-separation companion emerged from a shallow RV trend obtained with the Tull Spectrograph at the Harlan J. Smith telescope during the McDonald Observatory Planet Search Program (MOPS; Cochran & Hatzes 1993). We subsequently recovered a faint comoving companion with adaptive optics imaging using NIRC2 at Keck Observatory as part of the McDonald Accelerating Stars Survey (MASS), a follow-up high-contrast imaging campaign to identify the nature of these long-term radial accelerations (Bowler et al. 2018, 2021). HD 47127 B is located at a projected separation of $1''.95$ (52 au) and orbital motion is evident between 2017 and 2020. Based on its absolute H -band magnitude, HD 47127 B is expected to be a late-T dwarf. In Section 2 we describe our RV and imaging observations of HD 47127. Astrometric measurements, demonstration of common proper motion, and results of the orbital fit can be found in Section 3. Finally, HD 47127 B is discussed in the broader context of other benchmark substellar companions in Section 4.

2. Observations

2.1. Radial Velocities

A total of 118 high-resolution ($R \equiv \lambda/\delta\lambda \approx 60,000$) spectra were acquired between 2001 and 2021 with the Tull Coudé spectrograph (Tull et al. 1995) using the $1''.2$ slit at McDonald Observatory’s 2.7 m Harlan J. Smith telescope. A molecular iodine cell was mounted in the light path to measure RVs with respect to an iodine-free template following the procedure in Endl et al. (2000). The very small secular acceleration for HD 47127 was removed. Results are shown in Figure 1 and RVs are listed in Table 1. A clear linear trend is evident with a slope of $-1.93 \pm 0.08 \text{ m s}^{-1} \text{ yr}^{-1}$. After subtracting the linear fit, the rms of the residuals is 8.2 m s^{-1} , which is about twice the median RV uncertainty of 4.7 m s^{-1} . This suggests that HD 47127 is slightly active or that it could harbor an

additional inner companion. However, its Mount Wilson Observatory S -index is low; we find a value of 0.158 ± 0.012 from our Tull spectra, which was derived by first computing the McDonald S -index and then transforming it to the Mount Wilson system following Paulson et al. (2002). This is consistent with other activity measurements for HD 47127 (Wright et al. 2004; Isaacson & Fischer 2010) and is similar to the Sun at minimum activity as well as old field stars of the same spectral type (e.g., Saikia et al. 2018). A Lomb–Scargle periodogram of the RV residuals does not reveal any significant peaks, so it is unclear if the excess RV scatter originates from one or more inner planets or perhaps from a modest level of stellar activity.

HD 47127 was also targeted with the Hamilton Spectrograph as part of the Lick Planet Search (Fischer et al. 2014). Altogether 13 RVs were obtained between 1998 and 2007 with a median velocity precision of 3.3 m s^{-1} (Figure 1). We find a slope of $-1.9 \pm 0.3 \text{ m s}^{-1} \text{ yr}^{-1}$, which is similar to (but much less precise than) the trend from the McDonald RVs. The rms level of the residuals is 5.9 m s^{-1} .

2.2. Adaptive Optics Imaging

We obtained natural guide star adaptive optics images of HD 47127 with Keck/NIRC2 in its narrow camera mode on the nights of 2017 October 10 UT, 2020 December 31 UT, and 2021 January 22 UT. HD 47127 was centered behind the 600 mas diameter partly transparent coronagraph mask for all of the observations. Dome flats were taken at the start of each night.

The 2017 October data consists of a single H -band frame with an integration time of 10 s and one coadd taken at the end of the night as the sky was brightening. Conditions were photometric with excellent seeing ($0''.4\text{--}0''.5$) throughout the night. Two point sources were visible—one brighter object at $\approx 5''.6$ from HD 47127 (a background star) and a faint object embedded in the speckle pattern at $\approx 2''$ (HD 47127 B). The 2020 December data set consists of 11 H -band images each with a single coadd taken in vertical angle (pupil-tracking) mode. The total field-of-view rotation was $6^\circ.1$ for this angular differential imaging (ADI; Liu 2004; Marois et al. 2006) sequence. The 2021 January observations consist of an ADI sequence in K_S band taken over the course of about 45 minutes. Each image has an integration time of 2 s per coadd with 10 coadds, resulting in a total exposure time of 20 s per frame. Cloud cover and seeing were highly variable; out of 80 frames, 68 were retained resulting in a field-of-view rotation of 59° .

Image reduction and point-spread function (PSF) subtraction of the 2020 December and 2021 January ADI sequences follow the description in Bowler et al. (2015). Raw frames are cleaned of cosmic rays and bad pixels, bias subtracted, and flat fielded. Images are then registered using the measured position of the host star behind the coronagraph and PSF subtraction is carried out using the Locally Optimized Combination of Images algorithm (Lafrenière et al. 2007). The final processed frames are shown in Figure 2. A nearby point source is visible in the single H -band image from 2017 October and the processed H -band frame from 2020 December, but it is not present in the K_S -band data from 2021 January.

3. Results

3.1. Relative Astrometry and Photometry

3.1.1. 2017 October Observations

Aperture photometry is used to calculate the flux ratio of HD 47127 B for the single coronagraphic frame from 2017 October. A “raw” flux value comprising the source, the sky background, and the local PSF wing of HD 47127 is calculated using a circular aperture radius of 4 pixels (one diffraction width at $1.6 \mu\text{m}$) centered on the centroid position of the companion. To estimate the background flux at that location, 48 non-overlapping identical apertures are sampled at the same separation as HD 47127 B but distributed azimuthally around the host star while avoiding the six diffraction spikes as well as HD 47127 B. The mean and standard deviation of these apertures are adopted as the local background level (sky plus stellar PSF) to sample variations in the speckle pattern in the image, and the true flux of HD 47127 B is taken to be the raw flux minus the mean of these local background values. The flux of HD 47127 A (f_A) is determined using the raw aperture-summed flux of the host star ($f_{r,A}$), the background sky level of the image (s), and the coronagraph throughput (t_H) in H band of $0.099\% \pm 0.013\%$ ($7.51 \pm 0.14 \text{ mag}$) from Bowler et al. (2015) as follows: $f_A = (f_{r,A} + s)/t_H - s$. This applies a small correction to the primary flux to take into account the fact that the coronagraph is attenuating the star-plus-sky flux, not just that of the host star. We measure a contrast of $\Delta H = 12.5 \pm 0.6 \text{ mag}$ for HD 47127 B, which includes uncertainties in the coronagraph throughput and companion background levels.

Astrometry is computed using the centroid positions of the primary and companion. To estimate the positional uncertainty, we inject a 2D Gaussian with the same amplitude and standard deviation as HD 47127 B at each of the 48 azimuthally distributed positions around the host star mentioned above. We then attempt to recover the locations of each of the synthetic companions using the same centroid positional approach we used for HD 47127 B. The maximum of these measurements is 0.7 pixel, which we adopt as a conservative estimate of the uncertainty in our centroid measurements of the companion. Our final astrometry for the 2017 October data set (epoch 2017.774) is $\rho = 1''.970 \pm 0''.010$ and $\theta = 4^\circ.6 \pm 0^\circ.3$, which takes into account uncertainties due to random measurement errors, plate scale precision, distortion solution, and true north orientation (for the P.A. value) following Bowler et al. (2015).

3.1.2. 2020 December Observations

Astrometry and relative photometry for the 2020 December ADI sequence is determined using the negative companion injection approach described in Bowler et al. (2018). We did not obtain unsaturated frames to independently flux calibrate the deep sequence, so for a PSF model we adopt the median-combined H -band unsaturated image of the bright star 12 Psc from Bowler et al. (2021) taken on 2017 October 10 UT. The PSF model flux is normalized to the mean of the peak values of HD 47127 behind the mask. The PSF model amplitude, separation, and P.A. are then iteratively adjusted using the amoeba algorithm (Nelder & Mead 1965) to remove the signal of the companion in the processed image and minimize the rms in a circular aperture at the position of the companion. After taking into account the mask transmission and associated uncertainty, this results in a contrast of

HD 47127

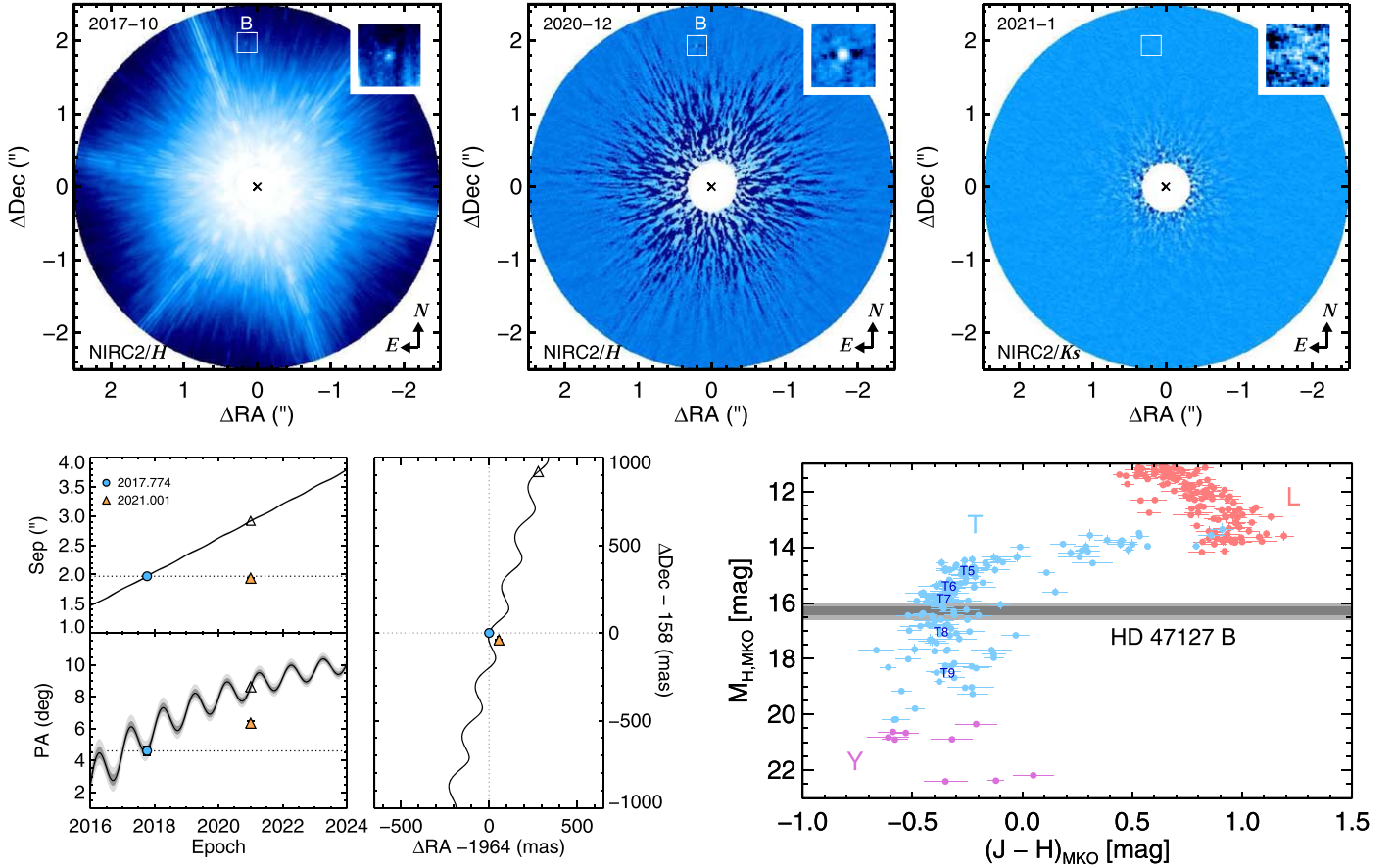


Figure 2. Upper panels: adaptive optics images of HD 47127 with Keck/NIRC2. In each observation the star (denoted with an “x”) is positioned behind the 600 mas diameter coronagraph. HD 47127 B is visible in a single raw H -band frame in 2017 October (upper left) and the PSF-subtracted H -band sequence in 2020 December (upper middle). We did not detect the companion in a K_S -band ADI sequence in 2021 January (upper right). The insets show zoomed-in views centered on the companion or its expected location, as in the case of the non-detection in 2021. North is up and east is to the left. Bottom left panels: expected trajectory of a background star (solid curve) relative to the initial astrometry in 2017 October (filled circle). Our second epoch in 2020 December (filled triangle) clearly establishes that HD 47127 B is bound with signs of orbital motion, especially in P.A. The open triangle shows its expected position if it was a background star. Bottom right panel: near-infrared color–magnitude diagram showing our 2020 December absolute H -band magnitude measurement of HD 47127 B compared to L, T, and Y dwarfs from The UltracoolSheet (<http://bit.ly/UltracoolSheet>). The gray shaded bands represent the 1σ and 2σ uncertainties. Based on this constraint, we expect HD 47127 B to be a late-T dwarf ($\approx T5$ – $T8$).

$\Delta H = 13.14 \pm 0.15$ mag—in agreement with our measurement from 2017 October at the 1σ level. Our best-fit astrometry for the 2020 December data set (epoch 2020.999) is $\rho = 1''.936 \pm 0''.003$ and $\theta = 6^\circ.34 \pm 0^\circ.16$, which also takes into account PSF blurring effects caused by field-of-view rotation within each exposure.

3.1.3. 2021 January Observations

HD 47127 B is not detected in our processed 2021 January data set, but a non-detection in K_S band nevertheless constrains the H – K_S color of the companion. A lower limit on the K_S -band contrast is determined using aperture photometry of the primary star and the rms counts at the location of the companion, which was determined from our 2020 December astrometry taken only a few weeks earlier. The average flux of the primary in a circular 4 pixel radius aperture from all 68 frames in the ADI sequence is adopted for the host. A correction is applied to take into account the $0.22\% \pm 0.02\%$ throughput of the 600 mas coronagraph mask from Bowler et al. (2015). Using a 3σ flux upper limit for the companion, we find a contrast of $\Delta K_S > 11.6$ mag. This implies that HD 47127

has an H – K_S color of < 1.7 mag based on the 2MASS magnitudes for the host.

3.2. Common Proper Motion

Figure 2 shows the expected motion of a background star relative to the initial astrometry from 2017 based on the proper motion and parallax of the host star from Gaia EDR3 ($\mu_\alpha \cos \delta = -74.864 \pm 0.028$ mas yr $^{-1}$, $\mu_\delta = -283.982 \pm 0.021$ mas yr $^{-1}$, $\pi = 37.561 \pm 0.025$ mas; Gaia Collaboration et al. 2021). A stationary background star should substantially increase in both separation and P.A. over time. HD 47127 B is clearly comoving with its host star and shows slight orbital motion, mostly in P.A. A linear fit to the orbital motion gives $\rho(t) = -10.5 \pm 3.2$ mas yr $^{-1}$ for the change in separation and $\theta(t) = 0^\circ.54 \pm 0^\circ.11$ yr $^{-1}$ for P.A.

3.3. Orbit Fit and Dynamical Mass

Astrometry of HD 47127 was obtained by both Hipparcos and Gaia, but does not show a significant acceleration in the Hipparcos–Gaia Catalog of Accelerations (HGCA) of

Brandt (2018). That catalog was based on Gaia DR2 and gives an acceleration of $d\mu_{\alpha\delta}/dt = 1.6 \pm 1.1 \text{ m s}^{-1} \text{ yr}^{-1}$, or a signal-to-noise ratio (S/N) of 1.5, using the Gaia and Hipparcos–Gaia scaled positional difference measurements following Brandt et al. (2019). More recently, Brandt et al. (2021) updated this catalog with Gaia EDR3.¹⁰ The proper motion differences in R. A. and decl. for HD 47127 are $\Delta\mu_{\alpha,\text{Gaia-HG}} = -0.12 \pm 0.05 \text{ mas yr}^{-1}$ and $\Delta\mu_{\delta,\text{Gaia-HG}} = 0.13 \pm 0.03 \text{ mas yr}^{-1}$, respectively. With this improved precision, HD 47127 shows a significant acceleration of $d\mu_{\alpha}/dt = -1.3 \pm 0.5 \text{ m s}^{-1} \text{ yr}^{-1}$ in R.A., $d\mu_{\delta}/dt = 1.4 \pm 0.3 \text{ m s}^{-1} \text{ yr}^{-1}$ in decl., and a total tangential acceleration of $d\mu_{\alpha\delta}/dt = 1.9 \pm 0.4 \text{ m s}^{-1} \text{ yr}^{-1}$ (S/N = 5.0). This is very similar to the RV trend of $1.93 \pm 0.08 \text{ m s}^{-1} \text{ yr}^{-1}$ from our Tull spectrograph observations. Together these tangential and radial accelerations define a three-dimensional acceleration vector, mapping out the reflex motion of the host star under the influence of a companion. Assuming this originates from the imaged companion HD 47127 B, this enables an orbit fit and direct dynamical mass measurement of this object.

The orbit and dynamical mass of HD 47127 B are constrained using the efficient Bayesian orbit fitting code *orvara* (Brandt et al. 2021). *orvara* incorporates absolute astrometry from HGCA, RVs (in this case from both McDonald and Lick), and relative astrometry and fits for nine parameters using Markov Chain Monte Carlo (MCMC): the primary mass (M_1), the companion mass (M_2), the orbital semimajor axis (a), two terms relating the eccentricity (e) and argument of periastron (ω)— $\sqrt{e} \sin \omega$ and $\sqrt{e} \cos \omega$ —the inclination (i), the longitude of ascending node (Ω), the longitude at reference epoch 2010.0 (λ_{ref}), and an RV jitter term added in quadrature with the measurement uncertainties (σ_{jit}). Other nuisance parameters such as the parallax, barycentric proper motion, and instrument-specific RV offsets are analytically marginalized out during the fits for computational efficiency. Priors in the fit are chosen to be broad or uninformative to avoid significantly influencing the posteriors. For the host mass we adopt a normal distribution centered at $1.02 M_{\odot}$ based on the constraint from Luck (2017) with a standard deviation of $0.10 M_{\odot}$, which is twice the uncertainty from Luck et al. to mitigate potential systematic errors in the isochrones used in that analysis. Log-uniform priors are adopted for the companion mass, semimajor axis, and RV jitter. The remaining priors are uninformative: $\sin i$ is used for inclination, and uniform distributions are chosen for $\sqrt{e} \sin \omega$, $\sqrt{e} \cos \omega$, Ω , and λ_{ref} . Eccentricities are bounded by $[0, 1)$, which is enforced by setting the prior equal to 0 if $(\sqrt{e} \cos \omega)^2 + (\sqrt{e} \sin \omega)^2 \geq 1$.

Results of the orbit fit are shown in Figure 3 and Table 2. The best-fitting orbit (as determined by the maximum likelihood) implies a semimajor axis of $74_{-22}^{+15} \text{ au}$, a modest eccentricity of $0.20_{-0.12}^{+0.45}$, an inclination of $62_{-10}^{+6} \text{ }^{\circ}$, and an orbital period of $610_{-270}^{+160} \text{ yr}$, although all parameter posteriors are generally very broad as a result of the small fractional orbital

coverage of the observations. The companion mass distribution is also broad and right skewed with a mode at $95 M_{\text{Jup}}$ and a median value of $105 M_{\text{Jup}}$. The 95.4% credible interval is $68\text{--}177 M_{\text{Jup}}$, which spans the stellar–substellar boundary at $\approx 78 M_{\text{Jup}}$. This immediately rules out the possibility that the companion is a white dwarf. The implications of this mass constraint are further discussed below.

4. Discussion and Conclusions

Compared to isolated brown dwarfs, a key advantage of brown dwarf companions is that their ages can be calibrated to that of their host star with the reasonable assumption that both components are coeval. With an age of 7–10 Gyr, HD 47127 B represents a rare instance of an old brown dwarf with an independent age constraint. At these ages, evolutionary models generally predict effective temperatures of $\approx 1300\text{--}2000 \text{ K}$ for masses at or just below the substellar boundary (e.g., Saumon & Marley 2008). This corresponds to spectral types spanning early-L to early-T, with the division between older stars and brown dwarfs occurring near L4 (Dupuy & Liu 2017). Brown dwarfs with even lower masses ($\lesssim 70 M_{\text{Jup}}$) should have cooled to T and Y dwarfs by the age of HD 47127.

We recovered HD 47127 B in a single filter but we can nevertheless broadly predict its expected spectral type using empirical relations between brown dwarf absolute magnitudes and spectral types. The H -band contrast from our 2020 December observations is $13.14 \pm 0.15 \text{ mag}$. The 2MASS H -band magnitude of HD 47127 is $5.28 \pm 0.03 \text{ mag}$ (Cutri et al. 2003), implying $H = 18.42 \pm 0.15 \text{ mag}$ and $M_H = 16.29 \pm 0.15 \text{ mag}$ for HD 47127 B.¹¹ This corresponds to a spectral type of $\approx \text{T7}\text{--}\text{T7.5}$ using the mean absolute magnitudes from Dupuy & Liu (2012). Using the less precise 2017 October contrast gives $M_H = 15.6 \pm 0.6 \text{ mag}$ and a spectral type of $\approx \text{T5}\text{--}\text{T8}$ (within 2σ). We therefore expect HD 47127 B to be a late-T dwarf, as illustrated in the near-infrared color–magnitude diagram in Figure 3. However, follow-up photometry and spectroscopy are needed to establish the spectral type and determine physical properties of HD 47127 B.

Compared to other benchmark T-dwarf companions, the H -band absolute magnitude of HD 47127 B is fainter than HR 2562 B, HD 13724 B, HD 19467 B, and Gl 229 B (which span $M_H = 14.2\text{--}15.6 \text{ mag}$), but brighter than Gl 758 B and HD 4113 C ($M_H = 16.7\text{--}18.2 \text{ mag}$). In terms of system architecture, HD 47127 B is perhaps most similar to HD 19467 B (Crepp et al. 2014): their host stars are both main-sequence solar analogs (with spectral types of G5 and G3 and masses close to $1 M_{\odot}$), the companions have mid- to late-T spectral types, and they orbit between 50 and 80 au.

The posterior mass distribution for HD 47127 B implies its mass is $>67.7 M_{\text{Jup}}$ with 99% confidence. However, HD 47127 B should be a T dwarf from its faint absolute magnitude and must therefore be below the hydrogen burning limit of $\approx 78 M_{\text{Jup}}$ (Burrows et al. 2001).¹² Assuming HD 47127 B is single and the only companion causing the observed acceleration, the best estimate for its mass is $67\text{--}78 M_{\text{Jup}}$ based on its dynamical mass and evolutionary models. Another possibility

¹⁰ In the Gaia EDR3 catalog, HD 47127 is listed as having a renormalized unit weight error (RUWE) = 1.131, $\chi^2 = 711$ (for 192 good AL observations), and astrometric excess noise = 0.14 mas. To assess whether these values are unusual for stars like HD 47127, we queried the Hipparcos catalog for bright G2–G5 main-sequence stars with $V = 6.3\text{--}7.3$ (within $\pm 0.5 \text{ mag}$ of HD 47127). This resulted in 398 stars, which were then cross-matched in Gaia. The median RUWE value, χ^2 value, and excess noise parameters are 1.03, 1032 (for a median of 316 good AL observations), and 0.129 mas, respectively. This suggests that the astrometric quality of HD 47127 in Gaia is typical for a star of this brightness.

¹¹ Note that no filter correction between H Mauna Kea Observatory (MKO) and H (2MASS) is applied for HD 47127 because this term is much smaller than the uncertainty in our contrast measurement.

¹² Note that the substellar boundary is a function of metallicity, helium fraction, and cloud opacity and can range from ≈ 73 to $84 M_{\text{Jup}}$ (see, e.g., Fernandes et al. 2019).

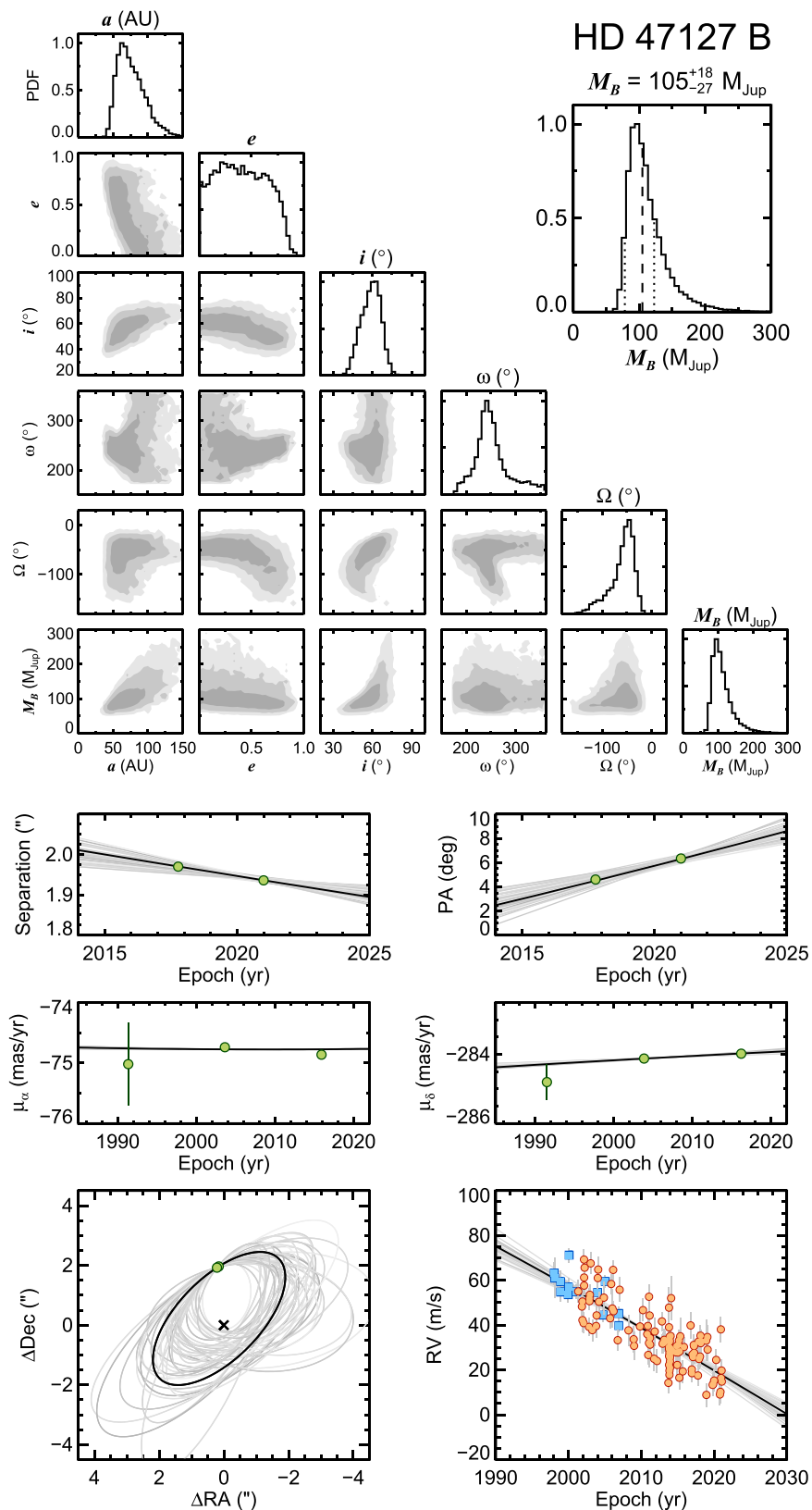


Figure 3. Results of the orbit fit for HD 47127 B. Top: corner plot showing the joint distributions of orbital elements and their marginalized distributions. The inset highlights the companion mass distribution, which is broad and allows for both stellar and substellar masses. If the true mass is near the median value of $105 M_{\text{Jup}}$, this would indicate the companion is itself a binary T dwarf or that an additional inner companion is biasing the observed acceleration. Bottom panels: randomly drawn orbits from the posterior MCMC chains compared to the relative astrometry; HGCA proper motions from Hipparcos, Gaia, and the scaled positional difference between the two missions; and RVs.

Table 2
HD 47127 B Orbital Fit Results

Parameter	Prior	Best Fit ^a	Median	MAP ^b	68.3% CI	95.4% CI
Fitted Parameters						
$M_1 (M_\odot)$	$\mathcal{N}(1.02, 0.10)$	1.0	1.02	1.03	(0.91, 1.12)	(0.82, 1.22)
$M_2 (M_{\text{Jup}})$	$1/M_2$	103	105	95	(78, 123)	(68, 177)
a (au)	$1/a$	74	73	65	(52, 89)	(44, 118)
$\sqrt{e} \sin \omega$	$\mathcal{U}(-1,1)$	-0.44	-0.51	-0.64	(-0.83, -0.30)	(-0.91, 0.15)
$\sqrt{e} \cos \omega$	$\mathcal{U}(-1,1)$	-0.06	-0.24	-0.35	(-0.54, -0.02)	(-0.61, 0.44)
i ($^\circ$)	sini	62	59	61	(52, 68)	(44, 72)
Ω ($^\circ$)	$\mathcal{U}(-180, 180)$	-41	-54	-49	(-71, -31)	(-117, -22)
λ_{ref} ($^\circ$) ^c	$\mathcal{U}(-180, 180)$	53	82	68	(35, 124)	(17, 205)
σ_{jit} (m s^{-1})	$1/\sigma_{\text{jit}}$	6.0	6.2	6.2	(5.5, 6.8)	(4.9, 7.5)
Derived Parameters						
e	...	0.20	0.40	0.33	(0.12, 0.65)	(0.0, 0.79)
ω ($^\circ$)	...	263	247	244	(216, 275)	(180, 334)
P (yr)	...	610	590	530	(340, 770)	(270, 1200)
τ (yr) ^d	...	2360	2240	2130	(2090, 2370)	(2080, 2810)
d_p (au)	...	59	43	21	(12, 66)	(7.3, 100)
d_a (au)	...	89	100	92	(78, 110)	(71, 150)

Notes.^a Maximum likelihood orbit.^b Maximum a posteriori probability, or mode of the marginalized posterior distribution.^c Mean longitude at the reference epoch, 2455197.5 JD.^d Time of periastron, $2455197.5 \text{ JD} - P(\lambda_{\text{ref}} - \omega)/(2\pi)$.

that could account for the unusually large maximum likelihood value of $103 M_{\text{Jup}}$ from our orbit fits is if HD 47127 B itself is a close unresolved binary, such as a pair of $\approx 50+50 M_{\text{Jup}}$ T dwarfs. Evolutionary models can be used to assess whether this binary hypothesis is plausible given the absolute magnitude and age of HD 47127 B. Cond models from Baraffe et al. (2003) predict that a single $50 M_{\text{Jup}}$ brown dwarf should have $M_H = 17.1$ mag at 8.5 Gyr and a range of $M_H = 16.8$ – 17.4 mag at 7–10 Gyr. An equal-flux binary would have $M_H = 16.3$ mag at 8.5 Gyr and $M_H = 16.0$ – 16.6 mag at 7–10 Gyr. This is in good agreement with the observed absolute magnitude of HD 47127 B, indicating that two equal-mass brown dwarfs could resolve the mass–absolute magnitude discrepancy. (Other binary mass ratios are of course also possible.) In this scenario HD 47127 B would resemble ϵ Indi Bab and Gl 417 BC, substellar companions that have been directly resolved into binaries. There are also hints that HD 4113 C may be an unresolved binary based on a discrepancy between the measured mass, spectral type, and age of the system (Cheetham et al. 2018).

It is also possible that another unseen close-in companion could be present in this system. The residuals of our McDonald RVs after subtracting the linear acceleration would imply a 3σ upper limit of 24.6 m s^{-1} for a velocity semi-amplitude. This corresponds to planet minimum masses of $m_p \sin i < \{0.3, 0.6, 0.9, 1.2, 2.0, 2.8\} M_{\text{Jup}}$ at orbital separations of $\{0.1, 0.5, 1, 2, 5, 10\}$ au, assuming circular orbits. Planets with minimum masses below that of Jupiter can be ruled out within ≈ 1.5 au. More massive planets and brown dwarfs can also reside at longer orbital periods if the observed radial and astrometric acceleration of HD 47127 is the superposition of multiple companions, as is suspected for the HD 206893 system (Grandjean et al. 2019).

HD 47127 B is poised to become an important addition to the short list of benchmark T-dwarf companions with orbits and

mass measurements. Additional relative astrometry of the companion and RV monitoring of its host will refine its eccentricity and mass, both of which are weakly constrained with our observations. HD 47127 B orbits at a moderately wide separation of $\approx 2''$, which makes it amenable to a wealth of follow-up studies including spin ($v \sin i$) measurements and atmospheric characterization. RVs of the companion can help constrain its orbit and mass, and high-resolution near-infrared spectroscopy with instruments like the Keck Planet Imager and Characterizer (Mawet et al. 2016) can be used to test the binary hypothesis by resolving multiple sets of lines. HD 47127 B will be an especially good target for imaging and spectroscopy with the James Webb Space Telescope to study its physical properties such as temperature, luminosity, surface gravity, and composition.











We thank Zhoujian Zhang and Michael Liu for helpful comments on this manuscript. We are grateful to Erik Brugamyer, Caroline Caldwell, Candace Gray, Kevin Gullikson, Bryce Hobbs, Marshall Johnson, Diane Paulson, Paul Robertson, Ivan Ramirez, Zili Shen, Andrew Vanderburg, and Rob Wittenmyer for contributing to the Tull observations of HD 47127 presented in this study. This work has benefited from *The UltracoolSheet*, maintained by Will Best, Trent Dupuy, Michael Liu, Rob Siverd, and Zhoujian Zhang, and developed from compilations by Dupuy & Liu (2012), Dupuy & Kraus (2013), Liu et al. (2016), Best et al. (2018), and Best et al. (2020).

This work was supported by a NASA Keck PI Data Award, administered by the NASA Exoplanet Science Institute. Data presented herein were obtained at the W. M. Keck Observatory from telescope time allocated to the National Aeronautics and Space Administration through the agency’s scientific partnership with the California Institute of Technology and the University of California. The Observatory was made possible

by the generous financial support of the W. M. Keck Foundation. B.P.B. acknowledges support from the National Science Foundation grant AST-1909209 and NASA Exoplanet Research Program grant 20-XRP20_2-0119. The authors wish to recognize and acknowledge the very significant cultural role and reverence that the summit of Maunakea has always had within the indigenous Hawaiian community. We are most fortunate to have the opportunity to conduct observations from this mountain.

Facilities: Smith (Tull Spectrograph), Keck:II (NIRC2).

ORCID iDs

Brendan P. Bowler  <https://orcid.org/0000-0003-2649-2288>
 Michael Endl  <https://orcid.org/0000-0002-7714-6310>
 William D. Cochran  <https://orcid.org/0000-0001-9662-3496>
 Justin R. Crepp  <https://orcid.org/0000-0003-0800-0593>
 Timothy D. Brandt  <https://orcid.org/0000-0003-2630-8073>
 G. Mirek Brandt  <https://orcid.org/0000-0003-0168-3010>
 Trent J. Dupuy  <https://orcid.org/0000-0001-9823-1445>
 Kaitlin M. Kratter  <https://orcid.org/0000-0001-5253-1338>
 Caroline V. Morley  <https://orcid.org/0000-0002-4404-0456>
 Yifan Zhou  <https://orcid.org/0000-0003-2969-6040>

References

- Ackerman, A. S., & Marley, M. S. 2001, *ApJ*, 556, 872
 Adams, W. S., Joy, A. H., Humason, M. L., & Brayton, A. M. 1935, *ApJ*, 81, 187
 Baraffe, I., Chabrier, G., Barman, T. S., Allard, F., & Hauschildt, P. H. 2003, *A&A*, 402, 701
 Baraffe, I., Chabrier, G., & Gallardo, J. 2009, *ApJL*, 702, L27
 Best, W. M. J., Liu, M. C., Magnier, E. A., & Dupuy, T. J. 2020, *AJ*, 161, 42
 Best, W. M. J., Magnier, E. A., & Liu, M. C. 2018, *ApJS*, 234, 1
 Bowler, B. P. 2016, *PASP*, 128, 102001
 Bowler, B. P., Blunt, S. C., & Nielsen, E. L. 2020, *AJ*, 159, 63
 Bowler, B. P., Cochran, W. D., Endl, M., et al. 2021, *AJ*, 161, 106
 Bowler, B. P., Dupuy, T. J., Endl, M., et al. 2018, *AJ*, 155, 159
 Bowler, B. P., Liu, M. C., Shkolnik, E. L., & Tamura, M. 2015, *ApJS*, 216, 7
 Brandt, T. D. 2018, *ApJS*, 239, 31
 Brandt, T. D., Dupuy, T. J., & Bowler, B. P. 2019, *AJ*, 158, 140
 Brandt, T. D., Dupuy, T. J., Li, Y., et al. 2021, submitted
 Burgasser, A. J., Geballe, T. R., Leggett, S. K., Kirkpatrick, J. D., & Golimowski, D. A. 2006, *ApJ*, 637, 1067
 Burrows, A., Hubbard, W. B., Lunine, J. I., & Liebert, J. 2001, *RvMP*, 73, 719
 Cheetham, A., Ségransan, D., Peretti, S., et al. 2018, *A&A*, 614, A16
 Cochran, W. D., & Hatzes, A. P. 1993, in ASP Conf. Ser. 36, Planets Around Pulsars, ed. J. A. Phillips, S. E. Thorsett, & S. R. Kulkarni (San Francisco, CA: ASP), 267
 Crepp, J. R., Johnson, J. A., Howard, A. W., et al. 2014, *ApJ*, 781, 29
 Currie, T., Brandt, T. D., Kuzuhara, M., et al. 2020, *ApJL*, 904, L25
 Cushing, M. C., Kirkpatrick, J. D., Gelino, C. R., et al. 2011, *ApJ*, 743, 50
 Cutri, R. M., Skrutskie, M. F., Van Dyk, S., et al. 2003, The 2MASS All-Sky Catalog of Point Sources (Washington, DC: NASA)
 Dupuy, T. J., & Kraus, A. L. 2013, *Sci*, 341, 1492
 Dupuy, T. J., & Liu, M. C. 2012, *ApJS*, 201, 19
 Dupuy, T. J., & Liu, M. C. 2017, *ApJS*, 231, 15
 Dupuy, T. J., Liu, M. C., & Ireland, M. J. 2009, *ApJ*, 692, 729
 Dupuy, T. J., Liu, M. C., & Ireland, M. J. 2014, *ApJ*, 790, 133
 Endl, M., Kürster, M., & Els, S. 2000, *A&A*, 362, 585
 Fernandes, C. S., Van Grootel, V., Salmon, S. J. A. J., et al. 2019, *ApJ*, 879, 94
 Fischer, D. A., Marcy, G. W., & Spronck, J. F. P. 2014, *ApJS*, 210, 5
 Gaia Collaboration, Brown, A. G. A., Vallenari, A., et al. 2021, *A&A*, 649, A1
 Glebocki, R., & Gnacinski, P. 2005, *yCat*, 3244, 0
 Grandjean, A., Lagrange, A.-M., Beust, H., et al. 2019, *A&A*, 627, L9
 Helling, C., Ackerman, A., Allard, F., et al. 2008, *MNRAS*, 391, 1854
 Isaacs, H., & Fischer, D. 2010, *ApJ*, 725, 875
 Kirkpatrick, J. D., Reid, I. N., Liebert, J., et al. 1999, *ApJ*, 519, 802
 Konopacky, Q. M., Ghez, A. M., Barman, T. S., et al. 2010, *ApJ*, 711, 1087
 Kumar, S. S. 1963, *ApJ*, 137, 1121
 Lafrenière, D., Marois, C., Doyon, R., Nadeau, D., & Artigau, É. 2007, *ApJ*, 660, 770
 Liu, M. C. 2004, *Sci*, 305, 1442
 Liu, M. C., Dupuy, T. J., & Allers, K. N. 2016, *ApJ*, 833, 96
 Liu, M. C., Dupuy, T. J., & Ireland, M. J. 2008, *ApJ*, 689, 436
 Luck, R. E. 2017, *AJ*, 153, 21
 Maire, A. L., Molaverdikhani, K., Desidera, S., et al. 2020, *A&A*, 639, A47
 Mamajek, E. E., & Hillenbrand, L. A. 2008, *ApJ*, 687, 1264
 Marleau, G. D., & Cumming, A. 2014, *MNRAS*, 437, 1378
 Marley, M. S., Fortney, J. J., Hubickyj, O., Bodenheimer, P., & Lissauer, J. J. 2007, *ApJ*, 655, 541
 Marois, C., Lafrenière, D., Doyon, R., Macintosh, B., & Nadeau, D. 2006, *ApJ*, 641, 556
 Mawet, D., Wizinowich, P., Dekany, R., et al. 2016, *Proc. SPIE*, 9909, 99090D
 Morley, C. V., Fortney, J. J., Marley, M. S., et al. 2012, *ApJ*, 756, 172
 Nelder, J. A., & Mead, R. 1965, *CompJ*, 7, 308
 Nordstrom, B., Mayor, M., Andersen, J., et al. 2004, *A&A*, 418, 989
 Paulson, D. B., Saar, S. H., Cochran, W. D., & Hatzes, A. P. 2002, *AJ*, 124, 572
 Rickman, E. L., Ségransan, D., Hagelberg, J., et al. 2020, *A&A*, 635, A203
 Saikia, S. B., Marvin, C. J., Jeffers, S. V., et al. 2018, *A&A*, 616, A108
 Saumon, D., & Marley, M. S. 2008, *ApJ*, 689, 1327
 Spiegel, D. S., & Burrows, A. 2012, *ApJ*, 745, 174
 Stanford-Moore, S. A., Nielsen, E. L., De Rosa, R. J., Macintosh, B., & Czekala, I. 2020, *ApJ*, 898, 27
 Tull, R. G., MacQueen, P. J., & Sneden, C. 1995, *PASP*, 107, 251
 Valenti, J. A., & Fischer, D. A. 2005, *ApJS*, 159, 141
 Wright, J. T., Marcy, G. W., Butler, R. P., & Vogt, S. S. 2004, *ApJS*, 152, 261